Supplementary Information

1 The vertical distribution of some basic environmental variables in the CM1 experiment

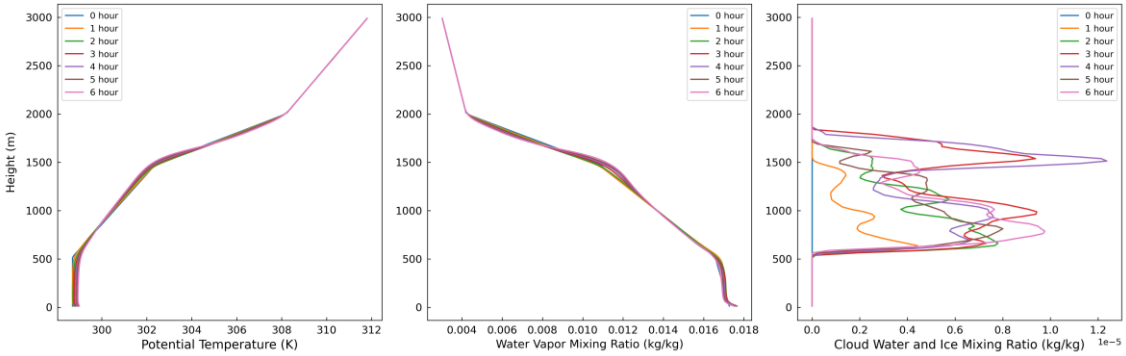

Figure S1. The temporal changes of the potential temperature, water vapor mixing ratio, cloud water, and ice mixing ratio with the height in the preliminary CM1 experiment.

Shallow cumulus convections commonly occur in the coastal areas, particularly around midday in the summer. Using the LES simulation in CM1, we simulated an ideal shallow cumulus convection weather condition and tracked the movement of air parcels under it. The vertical distributions of potential temperature and water vapor mixing ratio, as depicted in Fig. S1, exhibit relative stability, highlighting the differentiation between the boundary layer and the free troposphere. In this weather process, clouds and ice clouds gradually form between 500 m and 2000 m. Most of the tracked air parcels tend to move within 2000 m. As mentioned in the main text, approximately one-third of the air parcels ascend to altitudes exceeding 1000 meters, where cloud formation occurs. The ascent of air parcels is rapid, leading to significant environmental changes during this period. Temperature, pressure, and other information extracted from the CM1 simulation are utilized for subsequent PartMC-MOSAIC simulations.

2 Detailed changes in the chemical composition during the updraft period

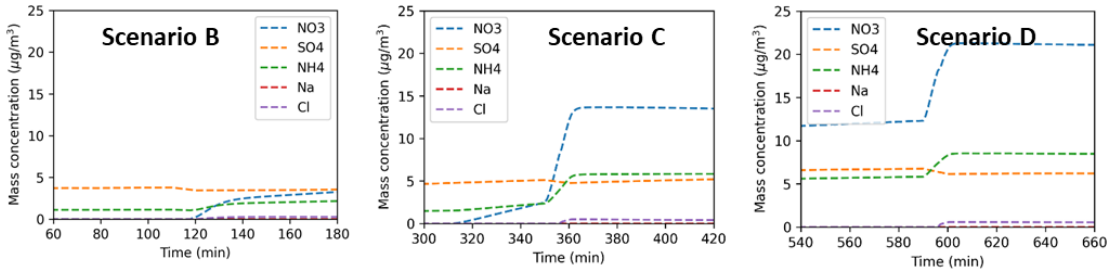

Figure S2. Mass concentration variations of the aerosol inorganic components during the two hours around the parcel updraft in Scenario B, Scenario C, and Scenario D.

In subsection 3.1, we presented the mass variations of aerosol chemical components in different scenarios. Due to the 24-hour simulation period, some high-resolution temporal changes may be lost in Fig. 1. In this part, we supplement the results by providing specific plots during the two hours surrounding the parcel ascent in Scenarios B, C, and D. As shown in Fig. S2, chemical compositions have undergone continuous changes over several minutes rather than a sudden change. The significant increase of nitrate and ammonium corresponds to the time when the parcel leaves the ground. The immediate ascent of the parcel has a large effect on the environmental factors, including temperature, pressure, relative humidity, and emission conditions.

In Scenarios C and D, the increasing trend of specific substances appears more intense than in Scenario B. This phenomenon is due not only to pollutant accumulation but also to the influence of solar effects. The changes associated with the sunlight are evident in the basic case, Scenario A, where the mass concentration of the nitrate rapidly increases after 11 a.m. Aside from the results in Fig. 1, the variation of related gases is also analyzed during the same period. Due to solar effects, the active oxidizing gas ozone may undergo significant changes during the daytime. In our background setup, the parcel in Scenario B departs the ground before 8 a.m., while the impacts of sunlight become apparent after 9 a.m. As a result, in Scenario B, the gases and aerosols remaining in the parcel could have a large difference from the ones in other scenarios.

3 The comparisons of number-size distribution

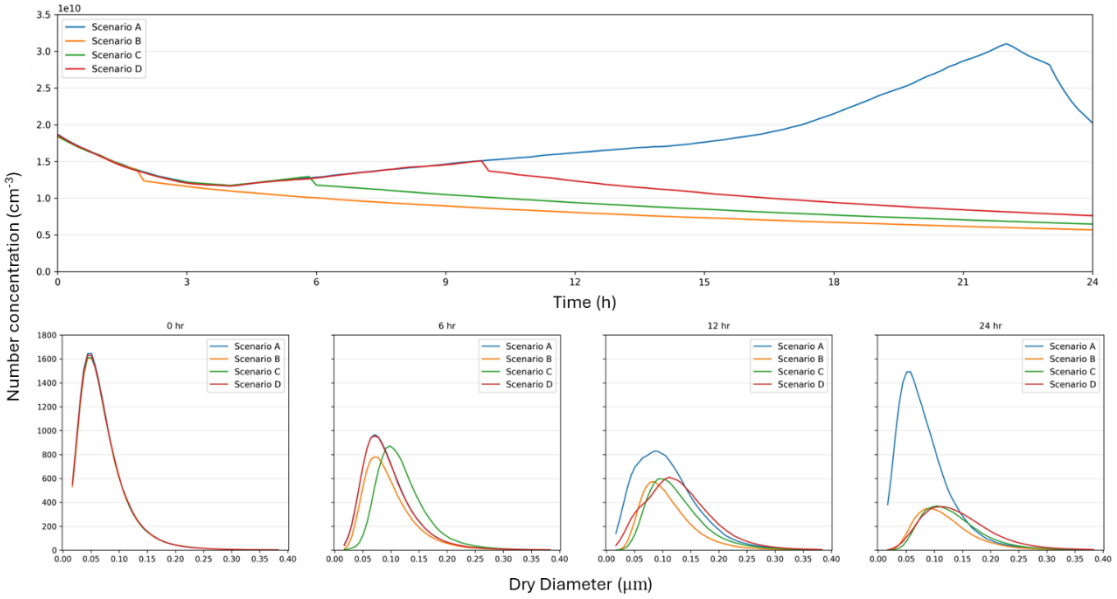

Figure S3. Time series of the total number concentration and the number size distribution of the particles at the selected time in Scenarios A, B, C, and D.

Figure S3 shows the temporal changes in the total number concentration and the size distribution in every scenario at the selected time. The blue, orange, green, and red curves represent the simulated number distributions for Scenario A, B, C, and D, respectively. It can be observed that in Scenario A, the total number concentration of the particles exhibits a descending trend until the 4th hour, after which it steadily increases until the 22nd hour. The descending period coincides with an elevation in the mixing height, indicating a more pronounced dilution effect. In the other scenarios, there is a small sharp decline in the total number concentration of particles during the rapid ascent of the parcel. This is because the parcel expands with the change in pressure and temperature, leading to a sudden decrease in the concentration of aerosols. Meanwhile, there are no longer emissions being introduced, and the surrounding aerosol concentration is also lower as these parcels ascend. Due to the cumulative effect of earlier emissions, the parcels that ascend later (Scenario D) have a higher concentration of particles. Under the combined effects of dilution, chemical reactions, and coagulation processes, the overall number concentration of particles is reduced after the updraft period. The mixing states of these three aerosol populations gradually approach stability, which is further discussed in section 4.

At the beginning of the simulation, the size of most of the particles is around 50 nanometers. The plot at the 24th hour demonstrates that in Scenario A, the particles are predominantly concentrated in the smaller size bins due to the continuous influx of emissions. Fresh emissions primarily consist of small particles, and subsequent aging processes contribute to an increase in both particle size and mass. When the parcels enter the high altitude, the growth regulation of the particle size

varies from the populations near the ground. Gas emissions provide the raw materials for gas-to-particle conversion processes for Scenario B, C, and D. Therefore, at the 12^{th} hour, it is evident that the dominating particles in the parcels with more residential time near the surface tend to have larger diameters. It becomes more prevalent that the size of the particles is around 100 nanometers.

60

4 The sensitive impacts of compositions on CCN activation

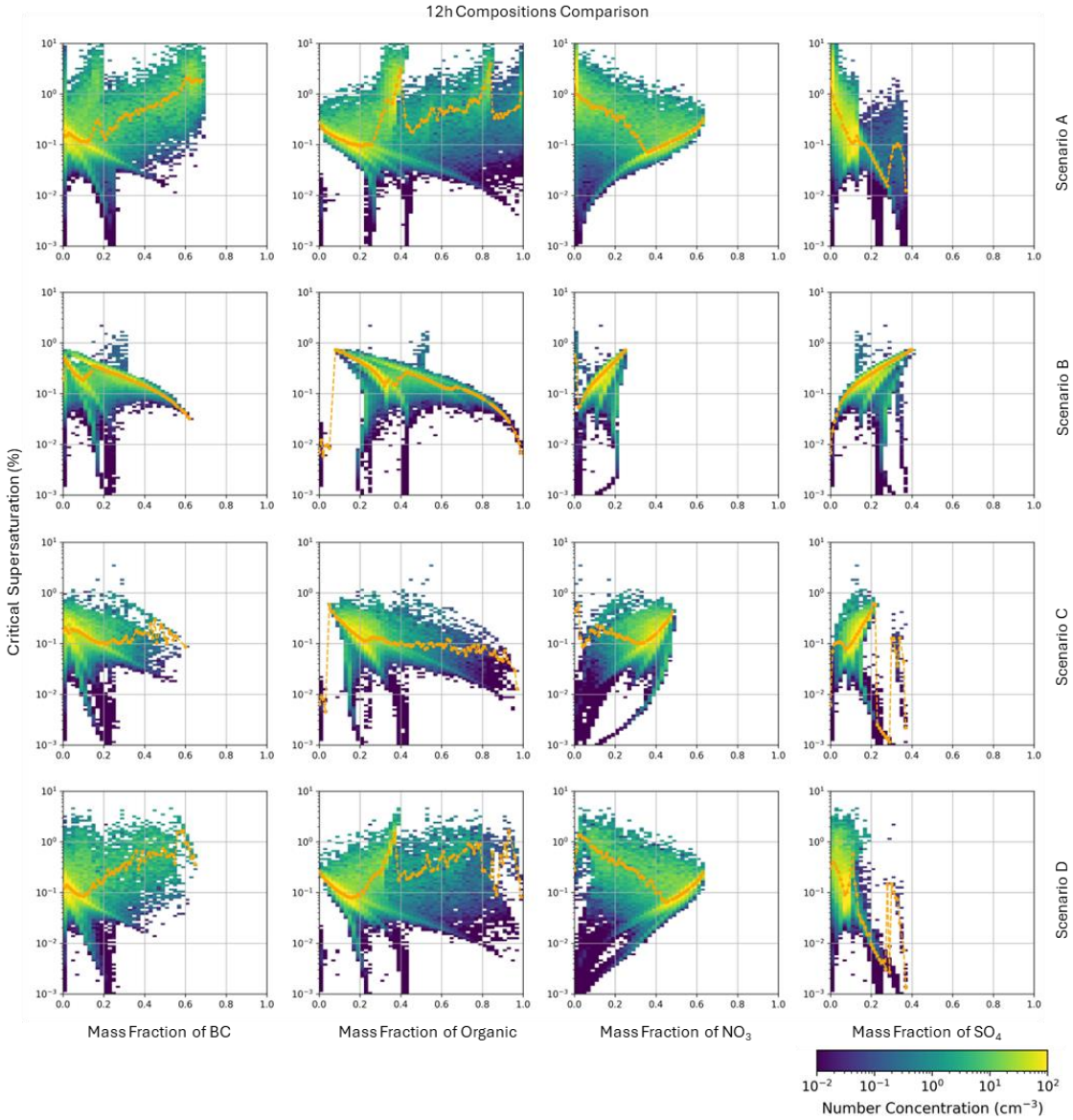

Figure S4. The relationship between the critical supersaturation and mass fractions of black carbon, nitrate, organic matter, and sulfate in aerosols. The figure shows the results for four scenarios on the 12th hour.

Figure S4 illustrates the relationship between the critical supersaturation and mass fractions of several main components in aerosol particles at the 12th hour. Different scenarios are shown in different rows and the color also represents the number concentration of the particles. The orange curves in every subplot depict the median value of the critical supersaturation versus the various mass fractions. In Scenario A, there are two predominant sub-populations with S_c values around 0.1 and 1.0,

respectively. In Scenario D, the S_c of most of the particles is around 0.1. The pattern observed in Scenario D resembles that of Scenario A, except for the second sub-population with a higher S_c. At this stage, the parcel of Scenario D has left the ground for about two hours and the discrepancy primarily arises from the continuous emissions in Scenario A. The distinct sub-population exhibits a low proportion of highly hygroscopic inorganic salt components, including sulfate and nitrate. The characteristics of freshly emitted aerosols are showcased, and they are not prominent in the other scenarios. It is indicated that the aging process may lead to an increased incorporation of inorganic salt components. The particles dominating in Scenario A display a considerable variation in S_c values. As a result, the difference in the CCN activity between the surface parcel and the actual parcel at higher altitudes is not consistently stable within the range of 0.1% to 1% supersaturation. At lower supersaturation levels, a greater number of particles may be activated in the surface parcel. Nevertheless, at higher supersaturation levels, such as 1%, the parcel at higher altitudes exhibits a higher degree of CCN activation.

The trend of the median S_c values (orange curves) reflects the variation in the activation potential of the aerosols as the mass fraction of different substances changes. In general, the S_c values of the particles tend to be lower when they are more prone to be activated. Previous studies have commonly attributed the high hygroscopicity of sulfate components as a key factor in CCN activation. However, the median curves fluctuate without a consistent tendency. With an increase in the mass fraction of sulfate in particles, Scenarios B and C exhibit a rising pattern in the median S_c values. This could be attributed to the influence of particle size. Not only the sort of component but also the size distribution determines the cloud-forming potential of the aerosol populations. Similar inconsistencies are observed in the results for hydrophobic compositions such as BC and organic matter. Despite the increase in mass fraction, the orange curves for organic matter do not exhibit an upward trend, especially for the predominant sub-populations. This finding challenges our conventional understanding. Although it has more organic matter content than other high-concentration aerosols, the particles located in the lower right corner of the yellow region demonstrate a relatively stronger activation potential due to the relatively larger particle sizes. The results may highlight the significant impact brought by the particle sizes. In Scenario B, C, and D, the maximum mass fraction of nitrate increases as the emission accumulates. Furthermore, excluding the freshly emitted particles in scenario A, the trend of the median curve remains uniform across the primary sub-populations in all scenarios. Contrary to expectations, particles with higher nitrate amounts exhibit lower capacity to be activated. This suggests that ammonium nitrate formed during the gas-to-particle conversion process may have a greater tendency to adhere to smaller particles.